 doi:10.20944/preprints202210.0274.v1

Article

Sliding Mode-based Traction Control System Design for Electric Scooter BLDCM through Field-Oriented Vector Control Approach

Caglar Uyulan[1]* and Ersen Arslan[2]

[1] Mechanical Engineering Department, İzmir Katip Celebi University, İzmir, Turkey
[2] E-micromobility Department, FIGES AS., Bursa, Turkey; ersen.arslan@figes.com.tr
*Corresponding author: caglar.uyulan@ikcu.edu.tr

Abstract: Nowadays brushless DC motors (BLDCMs) are becoming indispensable components as the electrification revolution in the mobility industry is happening. Electric kick scooters, so-called e-scooters, are among these micro-mobility vehicles which are powered by these motors. Due to the uncertain and nonlinear features, the controller performance developed for these motors degrades. For these reasons, a chattering-reduced cascaded Sliding Mode Control (SMC) scheme to effectively track reference motor speed in the outer loop by eliminating torque ripples in the inner loop current control was designed. Field-oriented Control (FOC) methodology was used to implement the SMC in the BLDCM. An exponential reaching law algorithm was proposed for sliding surfaces of the inner and outer loop controllers. The suitability and performance of electric scooter-hub motors were analyzed in terms of traction control. A cascaded speed and torque controller produced significantly favorable results representing minimized torque and current ripples, and operation over a wide speed range.

Keywords: Field Oriented Control (FOC); electric scooter; Traction Motor Control System; Sliding Mode Control

Highlights

- The Sliding Mode Control (SMC) scheme was employed to track reference motor speed and torque for an e-scooter.
- Brushless Direct Current Motor (BLDCM) was modeled in MATLAB Simulink environment with Field Oriented Control (FOC) method.
- The suitability and performance of the nonlinear SMC controller for e-scooter applications were discussed and demonstrated via featured simulation cases.
- The developed traction control system was found to be well-suited for usage in e-scooter applications.

Graphical Abstract

In this numerical study, a nonlinear control scheme has been designed to drive a BLDC hub motor of an e-scooter. The performance and suitability were checked on the system model of the motor with the FOC method.

Preprints (www.preprints.org) | NOT PEER-REVIEWED | Posted: 19 October 2022 doi:10.20944/preprints202210.0274.v1

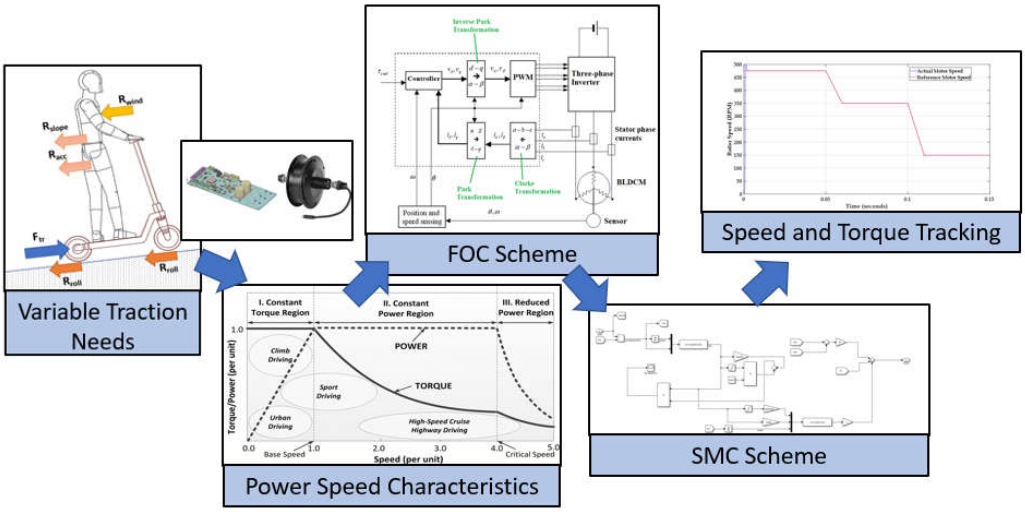

Figure. Graphical Abstract

Aim

This research aims to make a comprehensive study into the suitability of a nonlinear control method to drive a specific BLDC hub motor of an electric scooter from the point of view of traction.

Design & Methodology

A system modeling approach has been used to simulate the 48 V BLDC hub motor in the MATLAB Simulink environment. The Sliding Mode Control (SMC) scheme has been chosen to track the reference inputs(motor speed and motor torque) together with the Field-oriented Control (FOC) methodology for motor control.

Originality

The analysis of nonlinear schemes to drive a BLDC hub motor of an e-scooter has not been satisfactorily investigated in the literature. In this study, the SMC scheme has been investigated for a specific BLDC hub motor through a system modeling approach that can be utilized by the corresponding industry.

Findings

The suitability and performance of implementing an SMC scheme to drive a white-label electric scooter-hub motor was analyzed. A cascaded speed and torque controller produced significantly favorable results representing minimized torque and current ripples, and operation over a wide speed range.

Conclusion

The developed traction control system is well-suited for usage in electric scooter applications. The initial results are promising in a way that SMC can be employed for more efficient and stable driving compared to other linear schemes.

Declaration of Ethical Standards

The author(s) of this article declares that the materials and methods used in this study do not require ethical committee permission and/or legal-special permission.

 doi:10.20944/preprints202210.0274.v1

1. Introduction

With each passing year, the increase in the intensity of transport and the parallel increase in the emission amounts released increase the use of alternative drive systems. Studies conducted to overcome these problems show that electric vehicles that can be charged from a renewable source or the grid are the best solution. In the past, since the technical and financial problems in the storage of electrical energy could not be fully solved, electric vehicles could not replace internal combustion engine vehicles. At the same time, intensive research development (R&D) studies continue in areas such as performance, cost, reliability, and comfort.

When the studies on Electric Vehicles (EVs) are examined, it is seen that many types of research have been done in both automotive organizations and universities, and prototypes have been developed and commercially launched since the 1970s. Since the technical and financial problems of energy storage could not be fully solved in the past, such vehicles have never been able to replace internal combustion engine (ICE) vehicles [1-5].

After the 1990s, studies on alternative fuel vehicles started, especially with the breakdown of the ozone layer and global warming. In particular, fuel economy, decreasing oil resources and imbalances in prices, waste gas emission, limitations imposed by the European Union, and environmental and health factors have increased the research [6, 7].

The ability of Electric Vehicles (EVs) to store energy from renewable energy sources or the grid, and their low emission and environmental effects have made these types of vehicles stand out among alternative fuel vehicles. Today, while very sensitive variable speed values are required in electric vehicles, it is desired to be realized in a way that is reliable, cheap, robust, light and at the same time requires less maintenance [8-10].

Electric Scooters (ESs) have an electric motor and the technology to be connected directly to the electricity network with a socket. Electric scooters are two-wheeled vehicles that can be charged while slowing down, driving, braking, or plugging in from power plugs or specially separated power units at home and work. Electrically powered vehicles will not only draw energy from the electricity grid while they are being charged but will also be able to return additional energy to the grid during periods of high demand while parked. In this sense, the electric vehicle age will redefine driving habits while reshaping energy grids.

Soon, considering that consumers will be taxed according to the amount of carbon dioxide emitted from their vehicles, it is inevitable that energy-saving and environmentally-friendly electric vehicles will become more commercially viable. Today, with the advances in power electronics, semiconductor technology, permanent magnets, microprocessors and control, digital signal processing technologies, and collector and brushless, electronic commutated machines have been used in industrial applications. Especially the level that permanent magnet materials have reached in today's technology has caused permanent magnet motors to have an advantage over motors fed from the other two sides. Brushless DC Motors (BLDCM) are increasingly used in automotive, space technologies, computers, medical electronics, military, robotics, and household products due to their advantages such as high torque-power density, high efficiency, and reliability.

BLDCMs are electrical machines that perform energy conversion with the moment induced by the interaction of the conductor currents and the rotor permanent magnets' magnetic field. BLDCMs have many common features with conventional multi-phase alternating current motor structures. For ideal smooth and vibration-free continuous torque generation, the voltage and current excitation induced in the motor must be purely sinusoidal. In this type of motor, the stator windings around the air gap are sinusoidally distributed and the magnetic flux density produced by the rotor magnet changes to follow the sine function throughout the air gap. Sinusoidal phase currents are generated in such a way that the rotor angular position at every time is correct in synchronization with the supply phase currents. BLDCMs are fed through an inverter with the help of a high-sensitivity position sensor. In these motors, any disturbance that may cause phase currents or induced voltage to diverge from the sinusoidal waveform will cause the generation of

 doi:10.20944/preprints202210.0274.v1

unwanted moment vibration components. Therefore, high-sensitivity optical encoders or angle detectors are used for position detection. It is aimed to effectively control high efficiency and power density electric motors for an Electric Scooter (ES) that can be charged by using a plug-socket. The basic parts of an EV are the electric motor, motor drive circuit and controller, the battery group in which electrical energy is stored, and the charging system. If the problems in the implementation of this type of technology are examined: limited driving distance due to battery cost and short battery life. It is very important to select and design the electric motor and Drive and to develop control algorithms. When the electric motors used in the automotive industry and research are examined, it is seen that BLDCMs come to the fore. BLDCMs are preferred in the automotive field due to their superiority such as high torque/current and torque/inertia ratio, low volume and weight, robust structure, high efficiency, and reliability. In this context, being able to control the competitive, low-cost, efficient, and light BLDCM and Drive by the driving cycles of the ES is among the main objectives [11-14].

It is expected that high energy efficiency and low-cost, electric motor and drive systems will be developed for ES. Control of BLDCM and its Drive, parameter estimation, and optimization process will be performed together. The biggest problem with this type of motor technology is the high price of permanent magnets and their temperature sensitivity. This situation causes problems of high cost in mass production and a decrease in performance with temperature. Insulated Gate Bipolar Transistor (IGBT) will be used as a semiconductor switch element on the Drive level. High switching frequency, breakdown voltage, power capacity, operating temperature, and consequently high power density and losses are critical factors for drive efficiency. Space vector modulation (SVM) can be used to drive these semiconductor switches. Field-oriented control (FOC) strategy and also direct torque control (DTC) can be used under the control of the BLDCM. Position sensorless estimation methods (back-EMF or EKF-Extended Kalman Filter) will be used. As a controller, robust control methods, especially sliding mode control, will be used to provide the desired speed and current values [15, 16].

Sliding mode controllers (SMC) are quite effective in controlling non-linearities that occurred in the system, because of their ability to reject disturbances, invariant to parametric variations, and perform robust system performance. The SMC was implemented because of its operation attributes such as fast dynamics, robustness, stability-based disturbance rejection, variable structural control action, time-varying topology, etc. Mainly applied in the existence of modeling uncertainty, parameter variation, disturbances, parameter uncertainty, etc. [17, 18]. The effectiveness and superiority of the SMC over the standard classical linear control algorithms have been proven and discussed in the literature [19-22].

Since it is aimed to use a robust algorithm in a wide range along the low and high speed and variable load profile; the sliding mode control algorithm, which has advantages in this direction in terms of computation and accuracy, was utilized in this study. The rest of this paper is organized as follows. In Section 2, the traction motor selection for electric scooters was investigated. The mathematical model of the BLDCM and the FOC-based vector control approach were presented in Section 3 and Section 4, respectively. The SMC was designed in Section 5. The simulation results were demonstrated in Section 6. Finally, some conclusions are presented in Section 7.

2. Traction Motor Selection for Electric Scooter

The primary parameters and specifications are based on electric scooters widely used on the streets. The maximum scooter speed limit is 25 km/h, and a 0-20 km/h acceleration time of fewer than 4 seconds is acceptable for scooters used for transportation. The corresponding features of the investigated vehicle are given in Table 1.

Preprints (www.preprints.org) | NOT PEER-REVIEWED | Posted: 19 October 2022 doi:10.20944/preprints202210.0274.v1

Table 1. Primary parameters and performance specifications.

Primary Parameters	
Parameters	**Value**
Curb Mass	30 kg.
Gross Mass	105 kg.
Rolling Radius	127 mm.
Rolling Resistance Coefficient	0.005
Front Area	0.53 m2
Aerodynamic Drag Coefficient	0.79
Dynamic Performance Specifications	
Maximum Speed	25 km/h
0-20 km/h Acceleration Time	4 sec.
Maximum Gradeability (%)	20 (at 11.3 km/h)

It is very important to select and design the electric motor and drive system and to develop control algorithms. When examining the electric motors used in the automotive industry and academic research, BLDCMs come to the fore. The development of BLDCM technology and accordingly the design of speed measurement and estimation algorithms, real-time code and rapid prototyping, communication and integration of the control system with the existing equipment of the vehicle, the design and development of the drive with energy recovery braking, studies conducted by both academic and automotive companies continue [23-25]. This motor technology is increasingly used in Hybrid Electric Vehicles (HEVs) and EVs because of its advantages such as efficiency, power-torque density, lightness, and small volume, which are very important for EV technologies compared to other electric motor types.

Details on these comparisons are given in Table 2.

Table 2. A comparative table for electric motor technologies utilized in EVs.

Electric Motor Type / Criteria	*DCM*	*IM*	*PMSM*	*BLDCM*	*SRM*	*SynRM*	*PMa-SynRM*	*PM Hybrid*
Cost	0	++	-	-	+	++	+	0
Torque/Power Density	-	0	++	++	0	0	+	+
Efficiency	-	+	++	++	+	+	++	+
Simplicity/Manufacturability	++	++	+	0	++	++	+	-
Controllability	++	+	+	+	0	+	+	+
Reliability	-	++	+	+	++	++	+	+
Size/Weight/Volume	-	+	++	++	+	+	+	+
Overload Capability	-	+	+	+	+	++	++	++
Durability	0	++	+	+	++	++	+	+
Field Weakening Ability	++	++	-	+	++	++	++	0
Fault Tolerance	+	++	-	-	++	+	+	0
Thermal Bounds	0	+	-	-	++	++	+	-
Noise/Vibration/Torque Fluctuation	-	++	0	++	-	-	0	+
Life Span	-	++	+	+	++	++	+	+

*In this table: '+' Advantages, '-' Disadvantages, '0' indicates that there is no advantage or disadvantage) (The motor types in the table are; Direct Current Motor (DCM), Induction Motor (IM), Brushless Direct Current Motor (BLDCM), Switched Reluctance Motor (SRM), Synchronous Reluctance Motor (SynRM), Permanent Magnet Assisted Synchronous Reluctance Motor (PMa-SynRM), Permanent Magnet Hybrid Motor (PM Hybrid))

While industrial electric motors (EM) are selected and optimized for long and short-term load conditions, electric vehicles operate in a full torque-speed range and under variable driving conditions. Thus, it is essential to design a motor where the total lost energy in the driving cycle will be the smallest [26].

Preprints (www.preprints.org) | NOT PEER-REVIEWED | Posted: 19 October 2022 doi:10.20944/preprints202210.0274.v1

The selection of the electrical machine is very important when designing the whole system in an electric or hybrid vehicle. The EM design process for electric and mixed vehicles is based on the selection of the most appropriate geometric dimensions, taking into account criteria such as cost and weight. Charges, switching frequency, harmonic currents, losses, and flux orientation are critical in the design of the electric motor. Unlike conventional electric motors, electric motors and their drives designed for electric and mixed vehicles must provide the following characteristics [27-32]:

-High efficiency in the wide torque-speed range, especially for regenerative braking

-High power-torque density and huge initial torque, acceleration, and deceleration capacity

-Exerting high torque at low speeds (to increase travel and hill-climbing ability)

-Achieving high power at high speed

-Full-speed range comprising constant power and torque operating states

-Low speed on urban roads, high speed on the highway

-The highest speed is 4-5 times greater than the speed at the rated torque

-Easy application of field-weakening region

-Small scales

-Suitable for frequent starting and braking

-Sensitive voltage regulation

-Fast response

-Overload ability, usually doubles the rated torque

-Working with a high margin of error

-Durable control

-Lower costs

-Low maintenance

-Low noise

-Low torque ripple

-Low cooling requirement

-Technological sophistication and feasible structural integration

-Low electromagnetic interference and total harmonic distortion, etc.

Electric motor design and parameters for HEVs and EVs mostly depend on the vehicle's torque-speed characteristic and variable driving conditions. For any EM, size is always proportional to torque. The traditional torque-speed characteristic of an EM used in EVs and HEVs is given in Fig.1

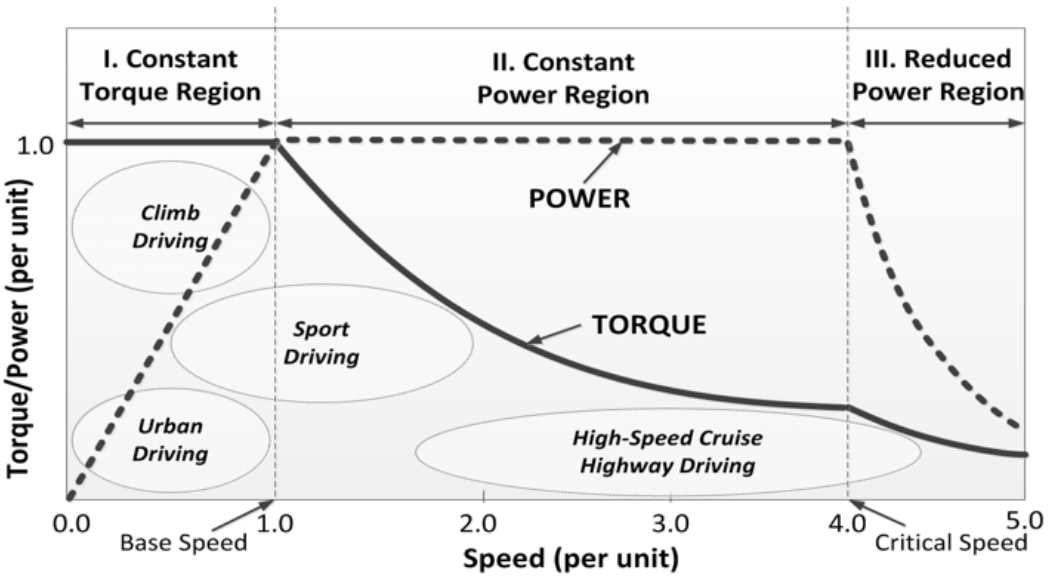

Figure 1. Ideal Torque / Power-Speed characteristics for electric vehicles [47].

Preprints (www.preprints.org) | NOT PEER-REVIEWED | Posted: 19 October 2022 doi:10.20944/preprints202210.0274.v1

For fast and smooth acceleration in the first region, the torque of EM must be constant at the highest value. The peak torque is limited by the motor current and temperature. A full-speed range is achieved by reducing the opposite EMF by using the flux attenuation technique. It is seen from the research that a variable speed range can be reached by varying the rotor structure, pole number, number of phases, and stator winding connection shapes. The second zone is the variable speed zone where the flux attenuation is performed. The third zone is the over-speed working zone that is used by reducing power requirements [33, 34].

To determine the specifications of the selected motor, the maximum motor power should be evaluated. The motor's peak power should compensate for the vehicle's maximum velocity, climbing performance of the vehicle, and 0-20 km/h acceleration time of the vehicle [35-38].

The power required for the vehicle to satisfy its maximum speed specification is given in Eq.1

$$P_{max,v} = \frac{1}{3600*\eta_t}\left(m*g*f*v_{max}\frac{C_D*A*v_{max}^3}{21.15}\right) \quad (1)$$

The power required for the vehicle to satisfy its climbing performance specification is given in Eq.2

$$P_{clb} = \frac{1}{3600\eta_t}\left(m*g*f*v_c*cos(\alpha_{max}) + m*g*f*v_c*\sin(\alpha_{max}) + \frac{C_D*A*v_c^3}{21.15}\right) \quad (2)$$

The power required for the vehicle to meet its 0-20 km/h acceleration time specification is stated in Eq.3

$$P_{acc} = \frac{1}{3600*t_m*\eta_t}\left(\delta*m*\frac{v_m^2}{7.2} + m*g*f*\frac{v_m}{1.5}*t_m + \frac{C_D*A*v_m^3}{21.15*2.5}*t_m\right) \quad (3)$$

where η_t is the driveline efficiency (power source to traction wheels); $m$is the mass of the vehicle (kg); g is the acceleration due to gravity (9.81 $\frac{m}{s^2}$); $f$is the rolling resistance coefficient of the tire; $C_D$is the aerodynamic drag coefficient; $A$is the vehicle front area (m²); v_{max} is the maximum velocity of the vehicle ($\frac{km}{h}$); α_{max} is the maximum grading angle of the vehicle (rad); v_c is the climbing/grading velocity of the vehicle ($\frac{km}{h}$); $\delta$is the rotational inertial factor of the vehicle; $t_m$is the specified 0-20 km/h acceleration time of the vehicle (s); $v_m$is the final acceleration speed ($\frac{km}{h}$), respectively.

The maximum power required for the traction motor can be stated as $P_{\max} \geq \max\left[P_{\max,v}; P_{clb}; P_{acc}\right]$.

The power (rated) specification of the motor can be found using the maximum power specification and the overload factor of the traction motor. The ability for the motor to be overloaded for short periods leads to a smaller motor selection. The power (rated) of the traction motor required can be evaluated as $P_{rated} = \frac{P_{\max}}{k}; P_{rated} \succ P_{\max,v}$ k is the overload factor.

The maximum speed specification of the motor can also be calculated from Eq.4

$$n_{\max} = \frac{v_{\max} * i_o}{0.377 * r} \quad (4)$$

where $i_0$is the gear ratio; r is the rolling radius.

The maximum torque of the motor can be evaluated using Eq.5 [39].

$$T_{\max} = \frac{9.55 * P_{\max}}{n} \quad (5)$$

where n is the rated motor speed.

Using Eq.1-5, the required traction motor specification is determined. The maximum speed required is approximately 2,7 times the base motor speed. The motor can be operated at speeds above its base speed implementing a motor control scheme having field-weakening to achieve the maximum speed requirement. Based on the evaluations, the required traction motor specifications are given in Table 3.

Preprints (www.preprints.org) | NOT PEER-REVIEWED | Posted: 19 October 2022 doi:10.20944/preprints202210.0274.v1

Table 3. Required traction motor specifications.

Specification	*Value*
Maximum Power	700 W
Rated Power	350 W
Rated Speed	478 RPM
Maximum Speed	620 RPM
Maximum Torque	32 Nm
Motor Overload Factor	1.9
Gear Ratio	Direct Drive

3. Mathematical Model of the BLDCM

BLDCM is a permanent magnet synchronous motor driven by an inverter by transforming dc-voltage into an ac-voltage. Most BLDCMs comprise rotors having rotor magnet pole pairs and three-phase stator windings. The stator windings induce an electromagnetic field and attract the stator field when the current is supplied. A proper current sequence determines the driving mechanism of the rotor magnets while the stator electromagnetic field is rotating. The electromagnetic field of the stator shares the same rotation speed as the rotor. The phase lead among the magnetic field of the stator and rotor generates sustainable torque. The rotor position should be accurately measured to provide a proper sequence of the stator current. BLDCMs are classified w.r.t the waveform of their back electromotive force (emf). The structural properties such as stator slots and coil distribution are the main cause of the various waveform shapes of stator coil back-emf while the rotor rotates. The generated torque in the rotor shaft is proportional to the summation of all phase current values on each phase. So, the outer loop torque control corresponds to the phase current control. Current control depends on the synchronization of stator-rotor flux and control signals of phase currents. A three-phase inverter is required to satisfy these tasks. To accomplish the synchronization, the controller selects that a certain set of gates is to be switched on and the remaining to be off according to the position of the rotor. The phase current value control is to regulate the time sequence of those gates to be opened [48-50].

The direct-quadrature (dq) model was utilized in this paper for reducing the three-phase model via coordinate transformation. dq model given in Eq.6 was preferred for superiority in the motor dynamic analysis and control system design.

$$\frac{di_q}{dt} = \frac{1}{L_q}\left(-Ri_q - \overbrace{n_p\omega_m}^{\omega_e} L_d i_d - k_e\omega_m + v_q\right)$$
$$\frac{di_d}{dt} = \frac{1}{L_d}\left(-Ri_d + \overbrace{n_p\omega_m}^{\omega_e} L_q i_q + v_d\right)$$
$$\tau_e \approx k_e i_q \quad (6)$$

where subscripts d and q highlight the direct and quadrature independent component of the variables, i is the stator current, v is the control voltage, R is the coil resistance, L is the coil inductance, ω_m is the rotor angular velocity, ω_e is the electrical phase velocity, n_p is the number of rotor permanent magnet pole pairs, τ_e is the electrical torque, k_e is the torque constant, respectively.

When the motor is run at the rated speed, the torque produced is proportional to the q-current component. The reference current (i_q) is evaluated from the reference torque of the outer loop controller. Since the direct axis current (i_d) is not affected by the torque production, it is required to keep it at approximately zero for improving energy efficiency. The reference current tracking can be achieved by implementing the field-oriented vector control approach.

Even though the $d-q$ coordinate model does not rely on the position of the rotor, measuring the rotor angle in real-time with high resolution or estimating with high accuracy is required for reliable controller implementation. It is possible to measure the rotor

Preprints (www.preprints.org) | NOT PEER-REVIEWED | Posted: 19 October 2022 doi:10.20944/preprints202210.0274.v1

flux by measuring the angular speed of the motor shaft because the number of pole pairs determines the number of electrical revolutions within one mechanical revolution.

The mechanical part can be derived by the differential equation as in Eq. 7

$$\tau_e = B\omega_m + J\frac{d\omega_m}{dt} + \tau_L \quad (7)$$

where is motor torque in Nm; is the rotor moment inertia, and is the load torque.

4. Field-Oriented Vector Control Approach

FOC is derived from the space vector projection of stator current components along two rectangular axes defined as direct (d) and quadrature (q), respectively. The main motivation behind the FOC is that it provides precise speed control in high power-to-weight ratio motors. The direct axis is oriented along the rotor magnetic field axis. FOC is separated into two control methods that are direct and indirect. While the direct one is based on rotor flux vector identification by measuring or estimating, the indirect one depends on the rotor flux vector determination through indirectly measuring the rotor mechanical angle. Phase currents are transformed into a two-axis ($d-q$) system via Clarke's transformation. The transformed two-axis coordinate system is aligned with the rotor magnetic flux by applying Park's transformation. The evaluated $d-q$ axis currents are fed back to the controller. By using the $d-q$ coordinate BLDCM model, the q −axis current determines the motor torque.

Given command torque τ_{cmd}, the desired q −axis current can be evaluated as $i_{q,cmd} = {}^{\tau_{cmd}}/_{k_e}$, and the desired d −axis current is set to zero, i.e. $i_{d,cmd} = 0$. The torque control is transformed into the current control. Then, the direct and quadrature axis voltages coming from controllers are translated back to the stationary reference frame ($\alpha-\beta$) using inverse Park's transformation. Finally, $\alpha-\beta$ reference frame values are converted back to the three-phase quantities as pulse width modulation (PWM) input.

The block diagram of the FOC scheme is represented in Fig.2

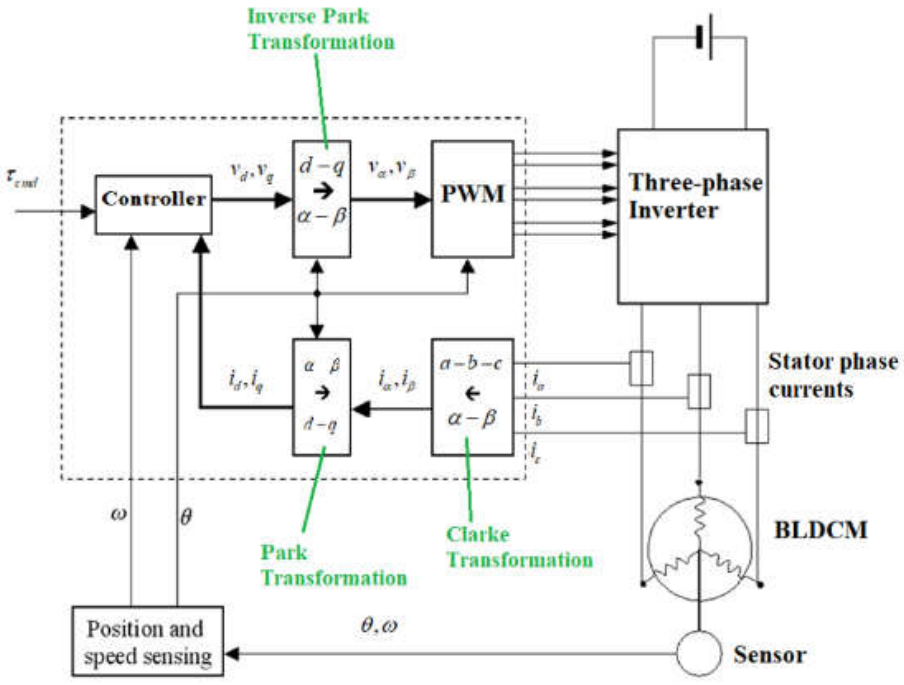

Figure 2. Block diagram of the FOC scheme.

The vector transformations are defined in Eq.8

Preprints (www.preprints.org) | NOT PEER-REVIEWED | Posted: 19 October 2022 doi:10.20944/preprints202210.0274.v1

$$\underbrace{\begin{vmatrix} i_\alpha \\ i_\beta \end{vmatrix} = \frac{2}{3}\begin{vmatrix} 1 & \cos\left(\frac{2\pi}{3}\right) & \cos\left(\frac{4\pi}{3}\right) \\ 0 & \sin\left(\frac{2\pi}{3}\right) & \sin\left(\frac{4\pi}{3}\right) \end{vmatrix}\begin{vmatrix} i_a \\ i_b \\ i_c \end{vmatrix}}_{Clarke-Transformation},$$

$$\underbrace{\begin{vmatrix} i_d \\ i_q \end{vmatrix} = \begin{vmatrix} \cos(\theta) & \sin(\theta) \\ -\sin(\theta) & \cos(\theta) \end{vmatrix}\begin{vmatrix} i_\alpha \\ i_\beta \end{vmatrix}}_{Park-Transformation}, \quad \underbrace{\begin{vmatrix} V_\alpha \\ V_\beta \end{vmatrix} = \begin{vmatrix} \cos(\theta) & -\sin(\theta) \\ \sin(\theta) & \cos(\theta) \end{vmatrix}\begin{vmatrix} V_d \\ V_q \end{vmatrix}}_{Inverse-Park-Transformation} \quad (8)$$

When a motor is used as the actuator, the input of the motor controller is a command torque (for the outer loop). Once the $d-q$ coordinate transformation was done, the motor torque is controlled via q-axis current as in Eq.9

$$i_{q,cmd} = \frac{\tau_{cmd}}{k_e} \quad (9)$$

At the same time, d-axis current is forced to near zero amplitude, in other words, $i_{d,cmd} = 0$. In practice, d-axis current can be utilized for identification purposes. Controlling torque is reduced to the current control problem where the desired current ($i_{q,cmd}$) depends on the torque command in the outer loop [40, 41].

To use a BLDCM as an actuator such as a traction motor, the electrical dynamics of the motor can be omitted as compared to the overall system dynamics. In another word, the controller and motor are accepted as a unitary feed-forward gain in the control loop [42]. Therefore, the feedforward inverse dynamics controller is applied to control d-current by considering the ideal knowledge of the plant and substituting Eq.6 back into the plant model. The closed-loop system dynamics are obtained in Eq.10

$$v_d = Ri_{d,cmd} - \omega_e L_q i_q$$
$$L_d \frac{di_d}{dt} = -Ri_d + Ri_{d,cmd} \quad (10)$$

5. Sliding Mode Controller Design

The sliding mode control (SMC) which originated from the variable structure control theory, is a discontinuous control method that considers the time-varying manifold. The SMC is preferable because of its main features such as agility, robustness, and stability-based disturbance rejection [43].

A sliding surface is specified in a way that the control action forces the system within the surface and hence, considers the desired system behavior. The reference torque required can be generated from the speed error. The exponential reaching law concept is utilized to compensate for the inner (current) and outer (speed) loops of the BLDCM. The system performance is modified continuously by switching the controlled variable concerning the current system state and thereby leading the trajectory to move on a sliding surface. The state trajectory begins in an arbitrary location on the phase plane and slides on the sliding surface. The sliding phase is defined as the phase in which the state trajectories change position towards the origin along this surface. As long as the system stays on this sliding surface, it remains unaffected by the changes in the system parameters and external disturbances. There exist two major tasks in the sliding mode design. First of all, a stable sliding surface should be chosen in the state space on which the state trajectories must stay. After that, a suitable control law must be designed to make reach the state trajectories to the sliding surface in a finite time [44-46].

The equation for constructing the sliding surface that guarantees the convergence of a variable to the reference value is given in Eq.11

$$S = \left(\frac{d(.)}{dt} + \alpha\right)^{n-1} e \quad (11)$$

where n is the system order, e is the tracking error signal, and α is a positive constant that regulates the system bandwidth.

The system order was two, and therefore the sliding surfaces for the current and speed controllers are evaluated as in Eq.12

$$S_i = \left(\frac{de_i}{dt} + \alpha_1 e_i\right)$$
$$S_\omega = \left(\frac{de_\omega}{dt} + \alpha_2 e_\omega\right) \quad (12)$$

Preprints (www.preprints.org) | NOT PEER-REVIEWED | Posted: 19 October 2022 doi:10.20944/preprints202210.0274.v1

where $e_i = i_{cmd} - i_q$; $e_\omega = \omega_{cmd} - \omega_m$; the subscript "cmd" refers to the reference signal; $\alpha_1$and α_2 constants.

The control law that makes reach the error to the sliding surface, should be built considering the criterion given in Eq.13

$$S_i\dot{S}_i \prec 0, S_\omega\dot{S}_\omega \prec 0 \quad (13)$$

The exponential reaching law is given in Eq.14

$$\dot{S}_i = -\varepsilon_1\, sgn(S_i) - \kappa_1 S_i$$
$$\dot{S}_\omega = -\varepsilon_2\, sgn(S_\omega) - \kappa_2 S_\omega \quad (14)$$

where κ_1 and $\kappa_2$are positive constants defined as hitting control gain or parameter; $\varepsilon_1$and $\varepsilon_2$are also positive constants; S is the sliding surface, and the sgn(.) function is stated as the signum function.

sgn(.) function causes the chattering phenomenon.

To reduce chattering, a boundary layer is proposed neighboring the sliding surface. sgn(.) terms in Eq.14 should be written as $sat(s/\Phi)$, where Φ is the thickness of the boundary layer and the saturation function can be given as $sat(x) = \begin{cases} x\ if\ |x| < 1 \\ sgn(x)\ if\ |x| \geq 1 \end{cases}$.

It can be understood that if $|s| \geq \Phi$, the system states shift to the sliding surface, when $|s| < \Phi$, the control changes linearly, and chattering is confined, but as an unwanted consequence, a steady-state error occurs. The smaller Φ causes less steady-state error but more serious chattering is observed, and vice versa.

Two cascaded controllers are utilized for the speed loop and current loop of the BLDCM. The outer loop controller aims to minimize the speed error converging the reference speed of the motor. The speed controller output is fed as input to the inner side current controller, which tries to minimize the current error by providing the motor to run at the required current.

The block diagram of the proposed SMC controller is given in Fig.3

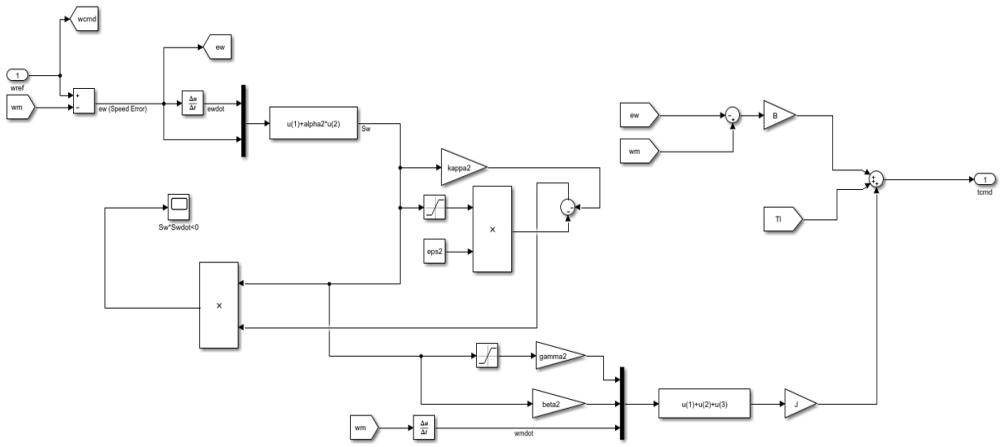

a)

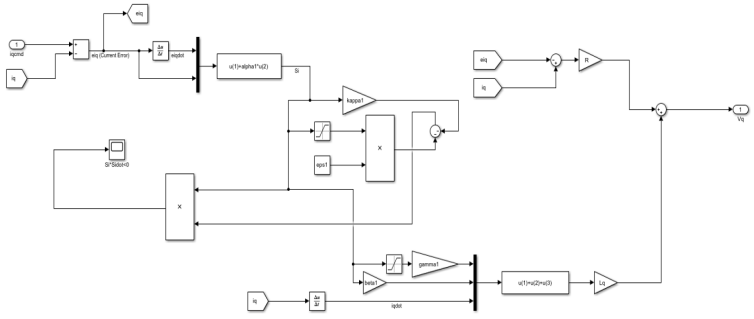

b)

Preprints (www.preprints.org) | NOT PEER-REVIEWED | Posted: 19 October 2022 doi:10.20944/preprints202210.0274.v1

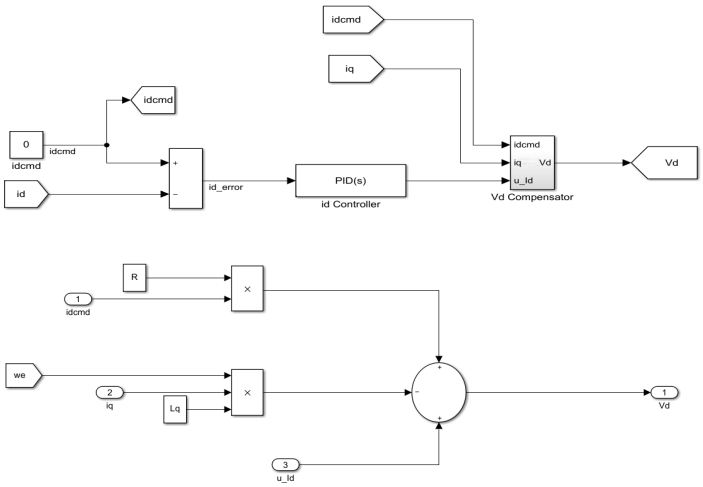

c)

Figure 3. Control scheme of the proposed SMC a) outer loop (speed control) b) inner loop (quadrature current control) c) inner loop (direct current control+Vd compensator).

The SMCs can be built by considering the exponential reaching law, and therefore the control signals τ_{cmd}, V_q are generated as in Eq.15

$$V_q = L_q\left(\gamma_1\, sgn(S_i) + \beta_1 S_i + \frac{di_q}{dt}\right) + (i_q - e_i)R_s$$
$$\tau_{cmd} = J\left(\gamma_2\, sgn(S_\omega) + \beta_2 S_\omega + \frac{d\omega_m}{dt}\right) + \tau_l + (\omega_m - e_\omega)B \quad (15)$$

where $\beta_1, \beta_2, \gamma_1, \gamma_2$ are constants.

The conditions stated in Eq.11 should be satisfied for every iteration in the simulation for the stability of the closed-loop control system. Therefore, the parameters must meet the "$\varepsilon_1, \varepsilon_2, \kappa_1, \kappa_2, \alpha_1, \alpha_2 \succ 0$" the inequality conditions. A closed-loop system is stable when all its eigenvalues have a positive real part. Incidentally, poles are the same as zeros. This means for stability, the number of zeros in the right half of the complex plane must be zero. A feedback control system is stable if all the roots of its characteristic equation have negative real parts (i.e. are to the left of the imaginary axis)

In addition, the direct current component was controlled through a feedback linearization PID control scheme.

6. Simulation Results

The BLDCM system and proposed sliding mode-based controller parameters are given in Table 4.

 doi:10.20944/preprints202210.0274.v1

Table 4. System and controller parameters.

System Parameter	*Symbol*	*Value*
Torque constant (electrical)	k_e	0.85
Torque constant (mechanical)	k_t	0.843
Rotational inertia	J	0.018 kgm^2
Coil resistance	R	0.225Ω
Coil inductance	L_d, L_q	0.00066 H
Viscous friction	B	0.05 Ns/m
Pole pair number	n_p	20
Controller Parameter	**Value**	
α_1	5316	
α_2	4624	
β_1	-20.55	
β_2	0.9761	
ε_1	19.55	
ε_2	0.00002	
γ_1	7.4877	
γ_2	14460	
K_1	14.023	
K_2	8.447	

The SMC controller parameters were optimized in the Simulink Response Optimization app by adjusting the design requirements as signal tracking. The criterion was chosen as the speed controller error was pulled to zero. A parallel pool was used during the optimization phase. The method and algorithm were selected as gradient descent, and sequential quadratic programming, respectively.

The simulation study of the SMC-controlled BLCDM was carried out in MATLAB-Simulink. The dynamic responses were investigated using the motor features given in Table 4. Initially, the motor was driven at no load at the rated speed of 478 RPM. After that, the pulse-shaped load was applied as 3 Nm at t=0.05 sec. with 0.01 sec. of period and 20% pulse width of the period. The reference motor speed was set as the rated speed (478 RPM). The speed variation of the rotor compared to the reference speed was demonstrated in Fig.4

Preprints (www.preprints.org) | NOT PEER-REVIEWED | Posted: 19 October 2022 doi:10.20944/preprints202210.0274.v1

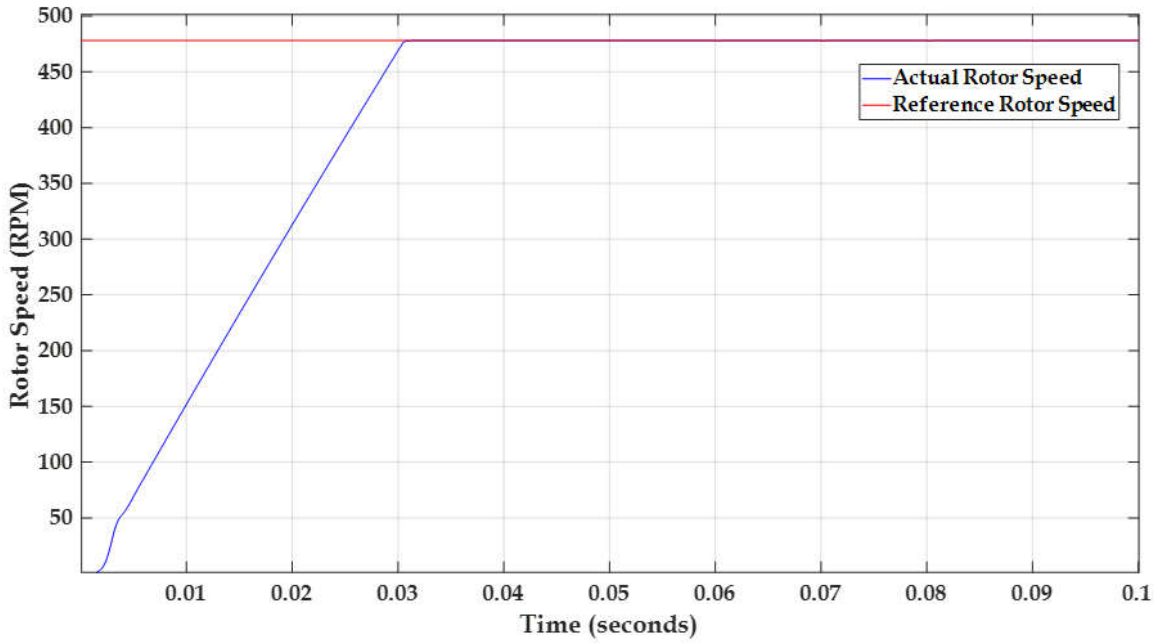

Figure 4. The rotor speed of 478 RPM of BLDCM for a pulse change in load at t=0.05 sec.

It can be inferred from the figure that the proposed SMC provides smooth operation and the load variation effects on the rotor speed are compensated.

The load torque, command torque, actual motor torque variations, and the direct current component (i_d) variations are depicted in Fig.5

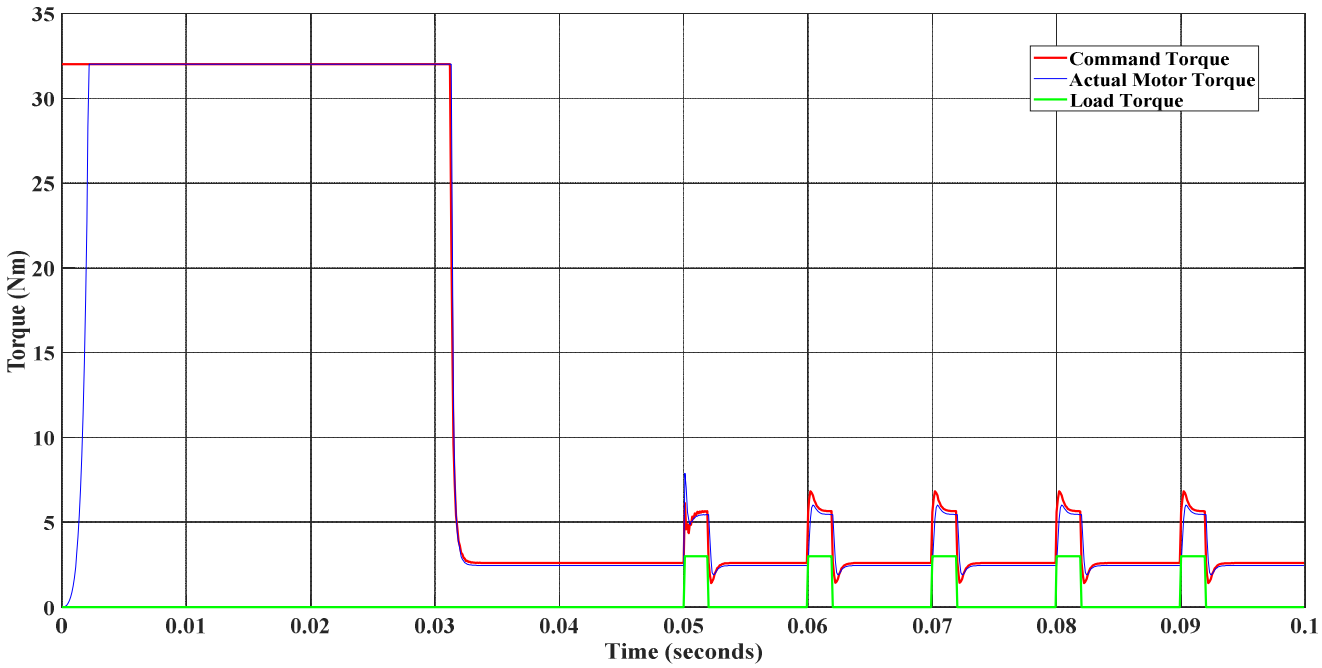

a)

Preprints (www.preprints.org) | NOT PEER-REVIEWED | Posted: 19 October 2022 doi:10.20944/preprints202210.0274.v1

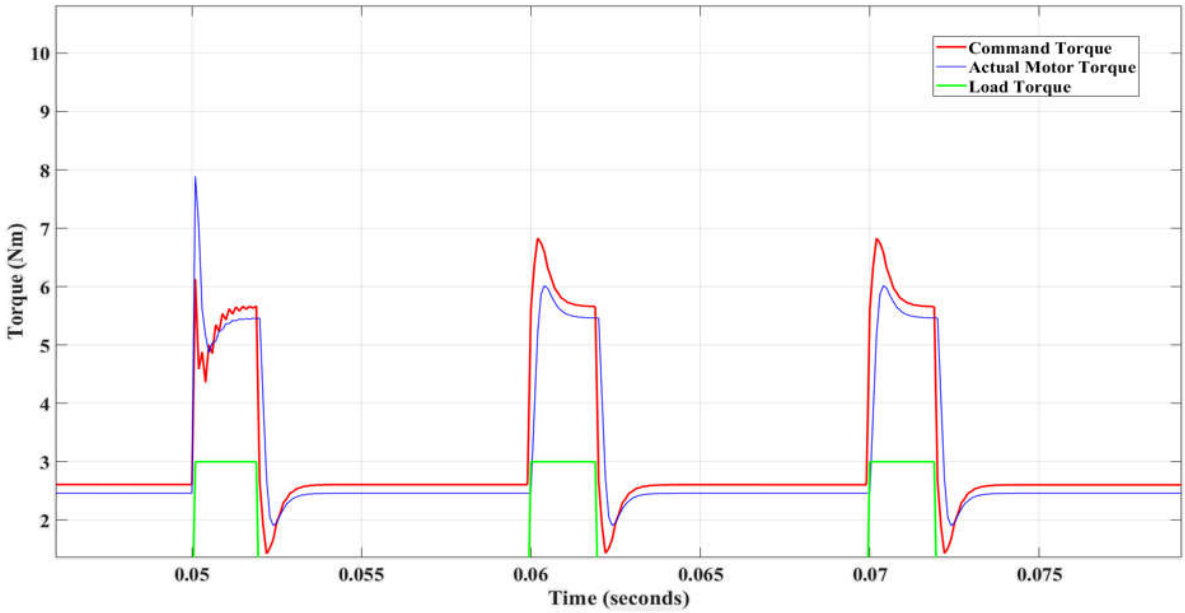

b)

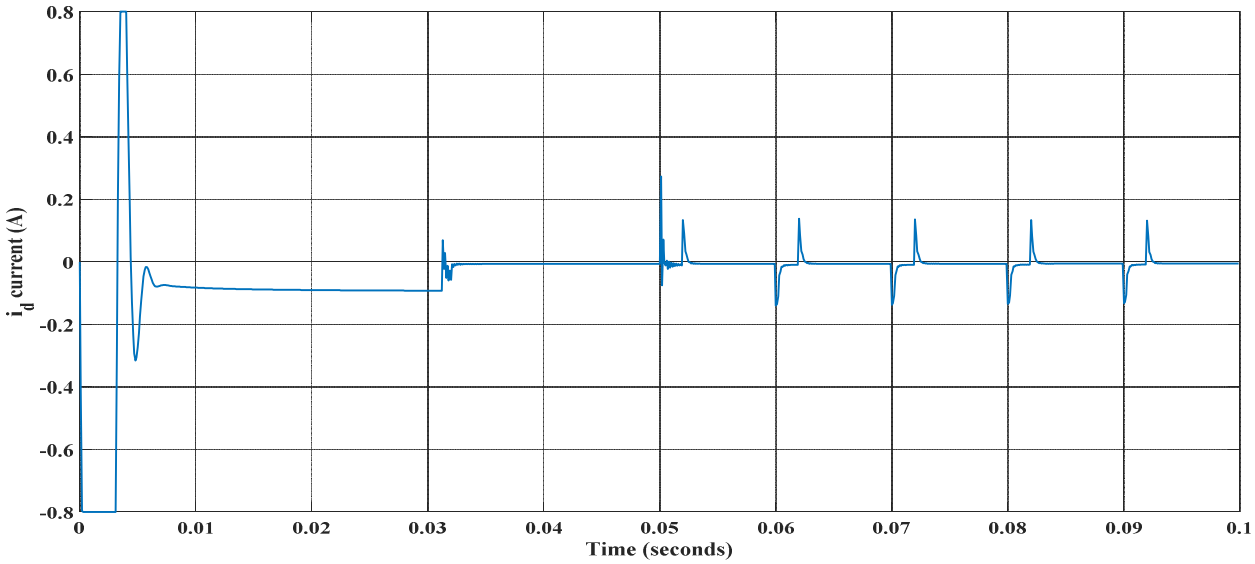

c)

Figure 5. a) Torque variations in the simulation. b) the zoomed version. c) i_d current variation.

The pulsations occur on the motor torque originating from the effect of the load torque, however, the proposed SMC reduces these chatterings. The vector control algorithm operated at the inner loop achieved good torque tracking.

The error dynamics of the speed and torque controller were depicted from time 0.05 sec. to 0.1 sec. in Fig. 6, respectively.

Preprints (www.preprints.org) | NOT PEER-REVIEWED | Posted: 19 October 2022 doi:10.20944/preprints202210.0274.v1

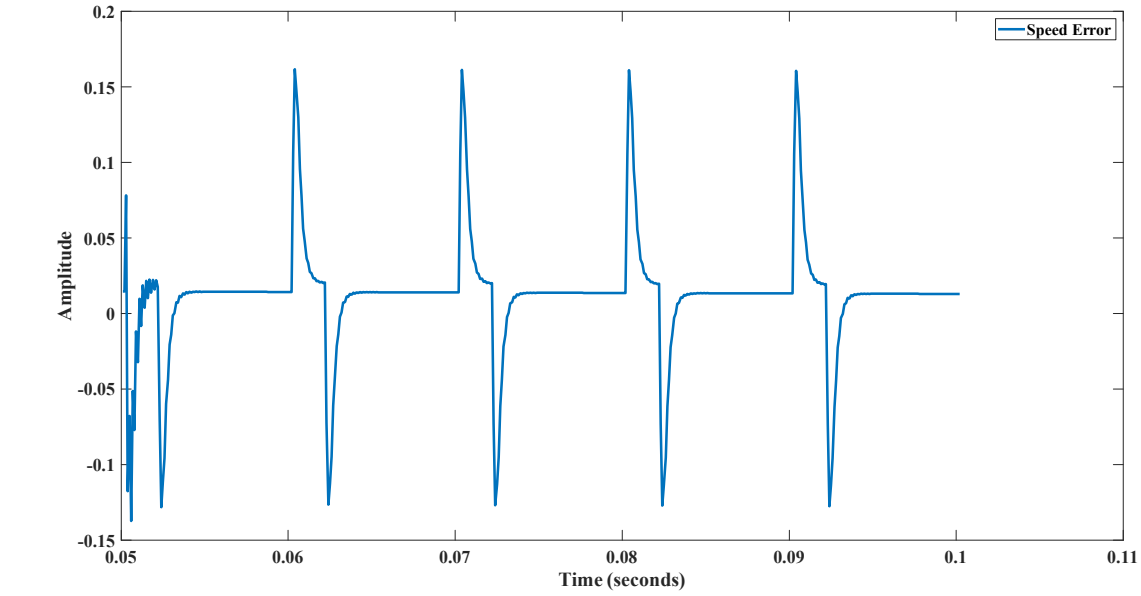

a)

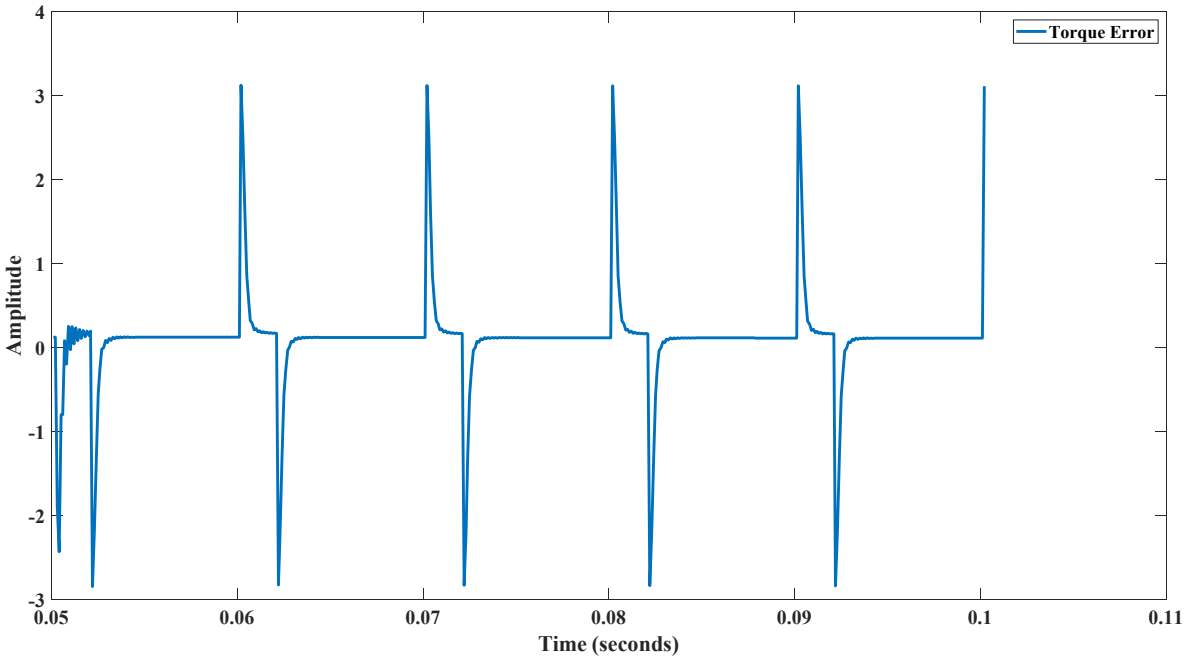

b)

Figure 6. The error dynamics of the a) speed controller and b) torque controller.

To evaluate the controller performance the error dynamics from 0.05 sec. to 0.1 sec. were taken into consideration using the root mean square metric (RMS). The RMS values were calculated as 0.6016 for the torque controller and 0.0394 for the speed controller, respectively.

The PI control scheme cannot handle the parameter variations and external force disturbance effectively. It has been seen a large steady error in the speed and torque responses obtained using the PI controller when the system parameter and load torque vary. According to the speed and torque error response with the two PI-based control schemes, the proposed SMC algorithm outperforms compared with the transient dynamic response and steady performance under large perturbations and parametric uncertainties. The

Preprints (www.preprints.org) | NOT PEER-REVIEWED | Posted: 19 October 2022 doi:10.20944/preprints202210.0274.v1

RMS values obtained from the speed and torque controller under the same simulation conditions were approximately 10 times higher as compared to the proposed SMC controller schemes, even if stability is ensured.

Another scenario covers the gradual changes in the speed reference signal. The motor is initially made to drive at 475 RPM and then the reference speed is decreased to 350 RPM, 150 RPM, and 0 RPM at time intervals of 0.05, 0.1, and 0.15 seconds. The variation of the speed in the motor is given in Fig.7

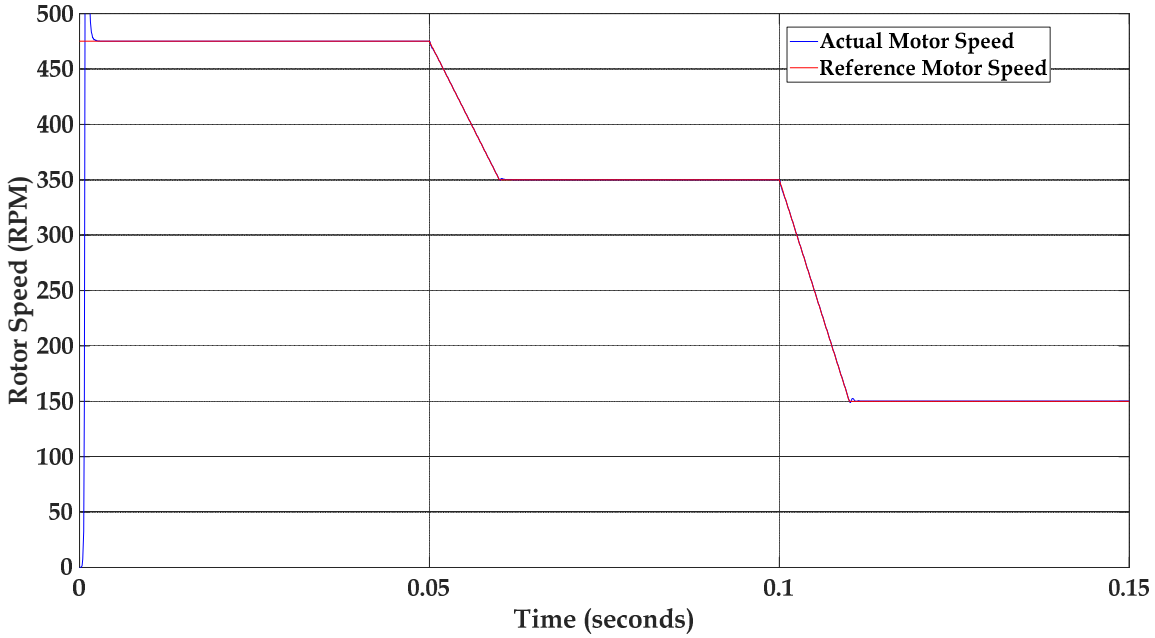

Figure 7. Speed tracking in BLDCM at no-load condition.

The error dynamics of the speed-tracking scenario are demonstrated in Fig.8.

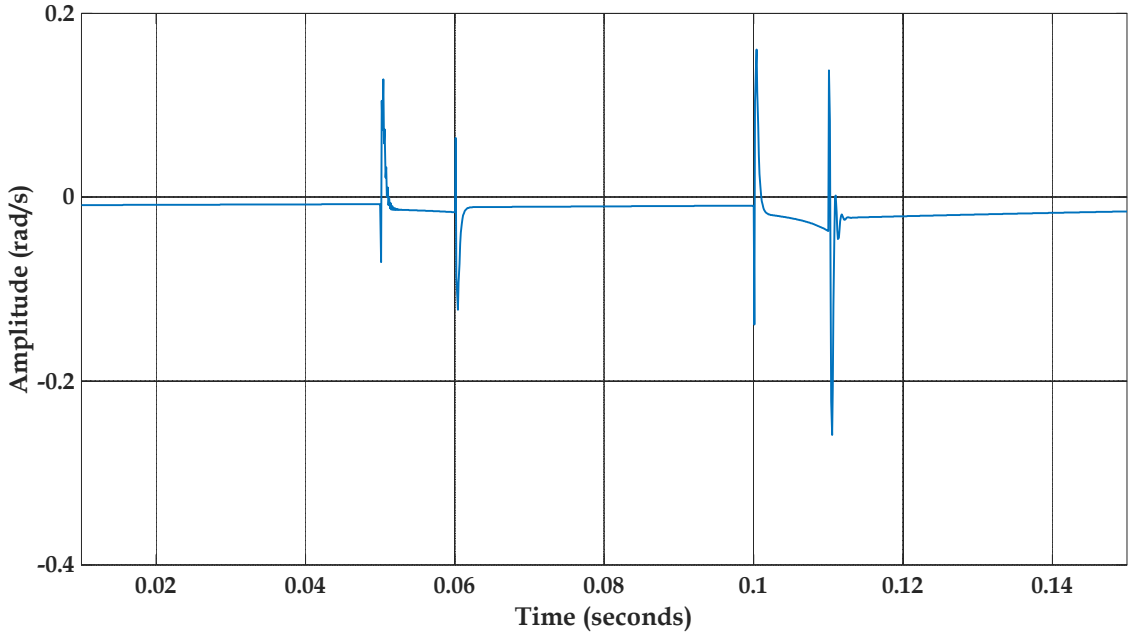

Figure 8. The speed tracking error is given from 0.01 to 0.15 seconds (the transient dynamics are omitted).

Preprints (www.preprints.org) | NOT PEER-REVIEWED | Posted: 19 October 2022 doi:10.20944/preprints202210.0274.v1

The proposed control methodology can track speed with the least variations.

Simulating the control system with scenarios that reflect the situations electric scooters may encounter would be more realistic and accurate. When considering terms of use, scooters are heavily exposed to the maximum load torque. For this reason, the last scenario includes the torque tracking under the condition of maximum load torque and the reference speed is near zero rpm. The simulation results are depicted in Fig.9.

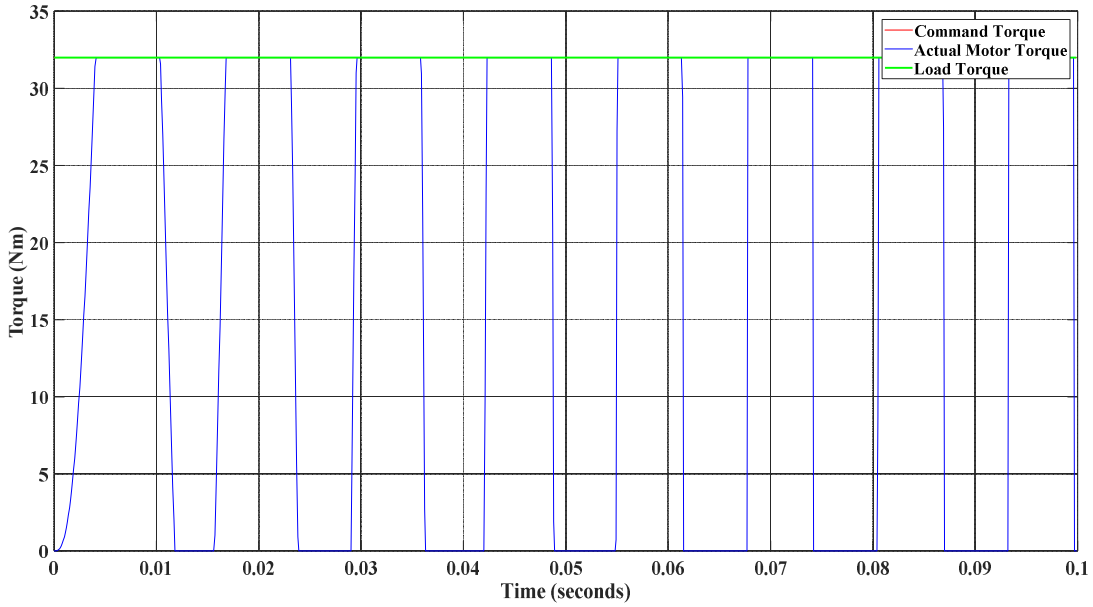

a)

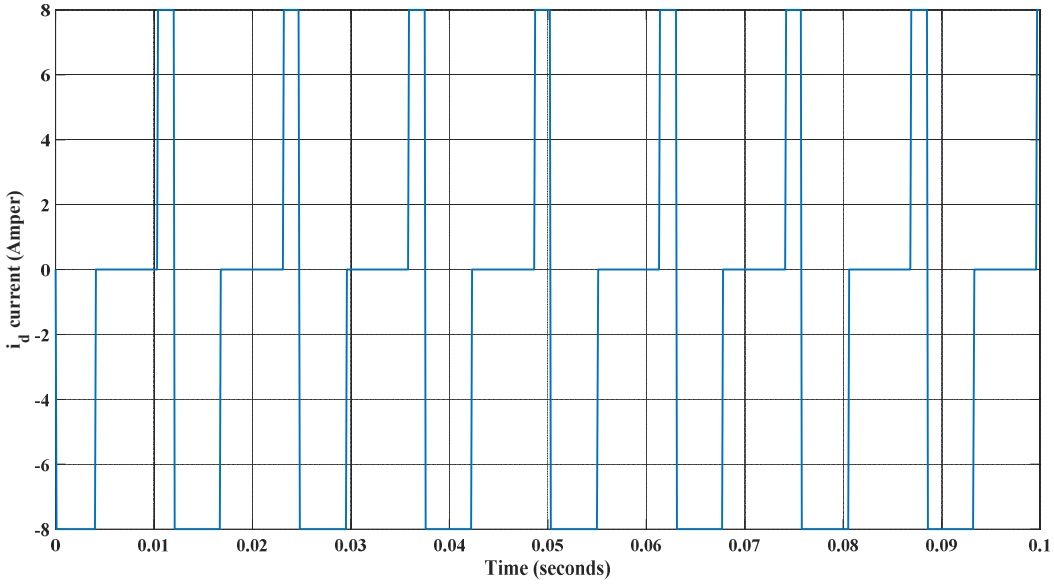

b)

Figure 9. a) Torque variations in the simulation. b) i_d current variation.

The time that actual motor torque reaches the load torque is approximately 4 milliseconds.

 doi:10.20944/preprints202210.0274.v1

7. Conclusion

SMC is an appropriate strategy to perform satisfactory control action for nonlinear systems. This paper combines the vector control approach with a modified SMC to perform effective speed and torque control for BLCDMs. The main advantage of the SMC from the conventional controllers (PID, Lead-Lag Compensator, LQR, State Variable Feedback Controller, etc.) is to provide improved performance under parameter variations, measurement noise, and enhanced speed response when the system is operated under load disturbances. The SMC combined with FOC provides important advantages such as confining the overshoot in speed, reducing steady-state error, and good dynamic response i.e. rapid rise time and settling time. The disadvantage of the SMC is that the produced control signal changes its direction too much which leads to a chattering phenomenon. It causes problems in practice such as component damage, fatigue, and unwanted energy consumption. Anyway, the commutation torque ripples can be reduced over the whole speed range using filtering, discontinuous approach, saturation function, etc. with a loss of robustness trade-off. From the results, it can be obtained that when the speed is gradually decreased, the BLDC motor mounted on the wheels of the scooter can be used effectively as a generator with regenerative braking. The proposed control scheme has a remarkable contribution in providing good control opportunities when we consider it with the direct-drive hub motor application used in electric scooters. Direct drive gives minimum relative moving parts, simplicity, and optimum package size. The proposed control methodology can also be applied to automation, robotics, position, and velocity control systems.

Acknowledgments: The authors would like to acknowledge the support of software and hardware infrastructures rendered by FIGES Inc.

References

1. Lowry, J., Larminie, J. 2012. Electric Vehicle Technology explained. Wiley.
2. Ehsani, M., Gao, Y., Longo, S., Ebrahimi, K. 2019. Modern electric, hybrid electric, and fuel cell vehicles. Boca Raton: CRC Press/Taylor & Francis Group.
3. Chan, C., Bouscayrol, A., Chen, K. 2010. Electric, Hybrid, and Fuel-Cell Vehicles: Architectures and Modeling. IEEE Transactions on Vehicular Technology, Vol. 59, s. 589-598.
4. Khayyam, H., Bab-Hadiashar, A. 2014. Adaptive intelligent energy management system of plug-in hybrid electric vehicle, Energy, Vol. 69, s. 319-335.
5. Kamichi, K., Yamamoto, M., Fushiki, S., Yoda, T., Kurachi, S., Kojima, K. 2012. Development of Plug-In Hybrid System for Midsize Car. SAE Technical Paper Series.
6. Aziz, M. 2017. Advanced Charging System for Plug-in Hybrid Electric Vehicles and Battery Electric Vehicles. Hybrid Electric Vehicles.
7. Luigi, F., Tarsitano, D. 2012. Modeling of Full Electric and Hybrid Electric Vehicles. New Generation of Electric Vehicles.
8. Sergaki, E. S. 2012. Electric motor efficiency optimization as applied to electric vehicles. International Symposium on Power Electronics Power Electronics, Electrical Drives, Automation and Motion.
9. Sha, L., Du, Q. 2011. Sensorless Control Technique for BLDCM. 2011 International Conference on Control, Automation and Systems Engineering (CASE).
10. Krishnan, R. 2017. Sensorless Control of PMBDCM Drive. Permanent Magnet Synchronous and Brushless DC Motor Drives, 555-560.
11. Gamazo-Real, J. C., Vázquez-Sánchez, E., Gómez-Gil, J. 2010. Position and Speed Control of Brushless DC Motors Using Sensorless Techniques and Application Trends, Sensors, Vol. 10, s. 6901-6947.
12. Zhang, Z. 2019. Robust Stator-Excited Brushless Synchronous Machine: An Attractive Permanent Magnet-Free Option. 2019 22nd International Conference on Electrical Machines and Systems (ICEMS).
13. Diab, H., Amara, Y., Hlioui, S., Paulides, J. J. 2021. Design and Realization of a Hybrid Excited Flux Switching Vernier Machine for Renewable Energy Conversion, Energies, Vol. 14, s. 6060.
14. Jayal, P., Bhuvaneswari, G. 2018. Vector control of permanent magnet synchronous motor drive using a reduced switch five-level inverter. IEEMA Engineer Infinite Conference (eTechNxT).
15. Kong, H., Cui, G., Zheng, A. 2010. Field-Weakening Speed Extension of BLDCM Based on Instantaneous Power Theory. International Conference on Electrical and Control Engineering.
16. Song, P. Y., Zhang, J. Y., Zhang, K. Y. 2010. Simulation of BLDCM Speed Control System Based on PI Controller with Fuzzy Parameter Regulators, Applied Mechanics and Materials, Vol. 29, s. 841-846.

17. Li, W., Wu, A., Wang, Y., Dong, N. 2016. Direct torque control for BLDCM based on optimized sliding mode observer. 12th World Congress on Intelligent Control and Automation (WCICA).
18. Il, K. G., Seung, H. M., Hak, Y. S., Cheol, L. Y. 2009. The study on BLDC motor compressor using SMC. IEEE 6th International Power Electronics and Motion Control Conference.
19. Shao, Y., Yang, R., Guo, J., Fu, Y. 2015. Sliding mode speed control for brushless DC motor based on sliding mode torque observer. IEEE International Conference on Information and Automation.
20. Hafez, A. T., Sarhan, A. A., Givigi, S. 2019. Brushless DC Motor Speed Control Based on Advanced Sliding Mode Control (SMC) Techniques. IEEE International Systems Conference (SysCon).
21. Alanis, A. Y., Munoz-Gomez, G., Rivera, J. 2020. Nested High Order Sliding Mode Controller with Back-EMF Sliding Mode Observer for a Brushless Direct Current Motor, Electronics, Vol. 9, s.1041.
22. Mohd Zaihidee, F., Mekhilef, S., Mubin, M. 2019. Robust speed control of PMSM using sliding mode control (SMC)—a review, Energies, Vol. 12, s. 1669. DOI: 10.3390/en12091669
23. Gu, D., Zhang, J., Gu, J. 2015. Brushless DC motor speed control based on predictive functional control. The 27th Chinese Control and Decision Conference (CCDC).
24. Qingchao, Z., Ruiqing, M., Junjun, D., Ben, Z. A cascade first and second order sliding mode control approach for speed control of brushless DC motor. 34th Chinese Control Conference (CCC).
25. Renken, F. 2010. Multiphase DC/DC converters for hybrid electric vehicles. Proceedings of 14th International Power Electronics and Motion Control Conference EPE-PEMC. DOI: 10.1109/epepemc.2010.5606634
26. Yilmaz, M. 2015. Limitations/capabilities of electric machine technologies and modeling approaches for electric motor design and analysis in plug-in electric vehicle applications, Renewable and Sustainable Energy Reviews, Vol. 52, s. 80–99. DOI: 10.1016/j.rser.2015.07.033
27. Umemura, C. 2001. Development of switched reluctance motor for EV traction system, SAE Technical Paper Series. DOI: 10.4271/2001-01-0957
28. Ying Fan, Chau, K. T. 2005. Design, modeling and analysis of a brushless doubly-fed doubly-salient machine for Electric Vehicles. Fourtieth IAS Annual Meeting. Conference Record of the 2005 Industry Applications Conference. DOI: 10.1109/ias.2005.1518843
29. Zarifyan, A., Zarifyan, A., Grebennikov, N., Talakhadze, T., Romanchenko, N., Shapshal, A. 2019. Increasing the energy efficiency of rail vehicles equipped with a multi-motor electrical traction drive. 26th International Workshop on Electric Drives: Improvement in Efficiency of Electric Drives (IWED). DOI: 10.1109/iwed.2019.8664283
30. Wu, H., Zhang, H. 2015. Model-based design and evaluation of Electric Vehicle Powertrain with independent driving motors. Volume 3: 17th International Conference on Advanced Vehicle Technologies; 12th International Conference on Design Education; 8th Frontiers in Biomedical Devices. DOI: 10.1115/detc2015-47980
31. Cheng, H., Wang, L., Han, G., Chen, H. 2019. The design and control of an electrified powertrain with switched reluctance machines for series Hybrid Electric Vehicle. IEEE Vehicle Power and Propulsion Conference (VPPC). DOI: 10.1109/vppc46532.2019.8952429
32. Rahman, K. M., Schulz, S. E. 2001. Design of high efficiency and high density switched reluctance motor for vehicle propulsion. Conference Record of the 2001 IEEE Industry Applications Conference. 36th IAS Annual Meeting (Cat. No.01CH37248). DOI: 10.1109/ias.2001.955916
33. Hayes, J. G., Goodarzi, G. A. 2018. Electric Powertrain: Energy Systems, Power Electronics and drives for hybrid, electric and Fuel Cell vehicles. John Wiley & Sons.
34. Bucherl, D., Nuscheler, R., Meyer, W., Herzog, H.G. 2008. Comparison of electrical machine types in hybrid drive trains: Induction Machine vs. permanent magnet synchronous machine. 2008 18th International Conference on Electrical Machines. DOI: 10.1109/icelmach.2008.4800155
35. Cheng, R., Dong, Z. 2015. Modeling and simulation of plug-in hybrid electric powertrain system for different vehicular application. 2015 IEEE Vehicle Power and Propulsion Conference (VPPC). DOI: 10.1109/vppc.2015.7352976
36. Lv, C., Zhang, J. 2011. Research of parameter design and matching of powertrain system in plug-in hybrid electric vehicle. International Conference on Electric Information and Control Engineering.
37. Zeng, X., Peng, Y., Song, D. 2014. Powertrain parameter matching of a plug-in hybrid electric vehicle. IEEE Conference and Expo Transportation Electrification Asia-Pacific (ITEC Asia-Pacific).
38. Kang, H., Dandan, Z. 2013. Study on Driving Motor of Pure Electric Vehicles Based on Urban Road Conditions. International Conference on Communication Systems and Network Technologies.
39. Pellegrino, G., Vagati, A., Boazzo, B., Guglielmi, P. 2012. Comparison of induction and PM synchronous motor drives for EV application including design examples. IEEE Transactions on Industry Applications, Vol. 48, s. 2322–2332. DOI: 10.1109/tia.2012.2227092
40. Kim, S. A., Byun, S. I., Cho, Y. H. 2015. A study on the advanced twelve step sensor-less control of BLDCM using FOC. Proceedings of the International Conference on Computer Information Systems and Industrial Applications. DOI: 10.2991/cisia-15.2015.49
41. Lianbing, L., Hui, J., Liqiang, Z., Hexu, S. 2009. Study on Torque Ripple Attenuation for BLDCM Based on Vector Control Method. Second International Conference on Intelligent Networks and Intelligent Systems.
42. Adiguzel, F., Turker, T. 2017. A switching adaptive current controller for BLDCM drives. 21st International Conference on System Theory, Control and Computing (ICSTCC).

43. Gadgune, S. Y., Waware, M. M. 2014. A novel control strategy for capacitor voltage regulation of Unified Power Quality Conditioner using Integral plus Sliding Mode Controller. International Conference on Circuits, Power and Computing Technologies [ICCPCT-2014].
44. Uyulan, C. 2019. A robust-adaptive linearizing control method for sensorless high precision control of induction motor. Measurement and Control, Vol. 52, s. 634–656. DOI: 10.1177/0020294019833072
45. Raisemche, A., Chaibet, A., Boukhnifer, M., Diallo, D. 2016. Mechanical sensor FTC using sub-optimal sliding mode observer for electrical vehicle induction motor drive. 13th International Multi-Conference on Systems, Signals & Devices (SSD).
46. Zhou, W., Zhang, X. 2016. Double closed loop sliding mode PID control system for BLDCM of pure electric vehicle. 35th Chinese Control Conference (CCC).
47. Vido, L., Amara, Y., Gabsi, M., Lecrivain, M., & Chabot, F. 2005. Compared performances of homopolar and bipolar hybrid excitation synchronous machines. Fourtieth IAS Annual Meeting. Conference Record of the 2005 Industry Applications Conference, 2005.
48. Adıgüzel, F., & Türker, T. 2022. A periodic adaptive controller for the torque loop of variable speed brushless DC motor drives with non-ideal back-electromotive force. Automatika, 63(4), 732–744.DOI:https://doi.org/10.1080/00051144.2022.2065802
49. Mohanraj, D., Aruldavid, R., Verma, R., Sathiyasekar, K., Barnawi, A. B., Chokkalingam, B., & Mihet-Popa, L. 2022. A review of BLDC Motor: State of Art, advanced control techniques, and applications. IEEE Access, 10, 54833–54869.DOI:https://doi.org/10.1109/access.2022.3175011
50. Kadhim, Q. S., Abbas, A. H., & Ali, M. M. 2022. Optimized speed control with torque ripple reductions of BLDC motor based on SMC approach using LFD algorithm. International Journal of Power Electronics and Drive Systems (IJPEDS), 13(3), 1305. DOI:https://doi.org/10.11591/ijpeds.v13.i3.pp1305-1314